Multiscale Modeling of High-Field Transport in 4H-SiC: A Novel Avalanche Generation Model Based on Full Band Monte Carlo Simulation

Mitsuhiro Sengoku
Advanced Semiconductor Device Development Center
TCAD Technology Development Dept.
Toshiba Electronic Devices & Storage Corporation
1 Komukai-Toshiba-cho, Saiwai-ku, Kawasaki, Kanagawa
mitsuhiro3.sengoku@glb.toshiba.co.jp

Souzou Kanie
Advanced Semiconductor Device Development Center
TCAD Technology Development Dept.
Toshiba Electronic Devices & Storage Corporation
300 Ikaruga, Taishi-cho, Ibo-gun, Hyogo
souzou.kanie@glb.toshiba.co.jp

***Abstract*—A novel avalanche generation model was developed using impact ionization coefficients calculated from high-field transport in 4H-SiC, utilizing multiscale modeling with DFT and FBMC.**

***Keywords*—DFT, Full Band Monte Carlo simulation, TCAD, multiscale modeling, 4H-SiC**

I. Introduction

4H-SiC, with its wide bandgap, allows for higher breakdown voltage designs compared to Si, making it suitable for next-generation power devices. Due to the significant anisotropy in the impact ionization coefficients of 4H-SiC, understanding this behavior is essential for designing high voltage devices. However, only the $\langle 0001 \rangle$ and $\langle 11\bar{2}0 \rangle$ directions have been experimentally reported, and no simulations have reported coefficients in arbitrary directions.

The Full Band Monte Carlo (FBMC) simulation is a versatile method for predicting electron transport in reciprocal and mesoscopic scale real space. Density Functional Theory (DFT) is commonly used for global energy band calculations, predicting material properties based on quantum mechanical atomic-scale physics.

In this study, we developed FBMC code and a novel avalanche generation model for 4H-SiC. The impact ionization coefficients along the $\langle 0001 \rangle$ and $\langle 11\bar{2}0 \rangle$ directions were reproduced using FBMC to ensure consistency with previous experiments, and the impact ionization coefficients in arbitrary directions were then predicted. These results were applied to Technology Computer-Aided Design (TCAD), enabling microscale device design for breakdown voltage optimization, based on physical insights derived from atomistic and mesoscopic scale modeling.

II. Simulation Method

Structural relaxation and self-consistent field (SCF) calculations were performed using the Quantum ESPRESSO package [1], employing ONCV pseudopotentials [2] and the PBE exchange-correlation functional. A plane-wave cutoff energy of 90 Ry and a k-point mesh of 32×32×8 were used. The results were used to generate Maximally Localized Wannier Functions (MLWFs) using Wannier90 [3] to interpolate the electronic band structure including up to 40 bands on a 96×96×24 k-point grid in the Brillouin zone.

In the FBMC, intravalley and intervalley scattering, polar optical phonon (POP) scattering, ionized impurity scattering, and impact ionization were considered. The scattering rate is set as inverse of momentum relaxation time and given by

$$\frac{1}{\tau_{\mathrm{ac}}} = \frac{\pi D_{\mathrm{ac}}^2 k_{\mathrm{B}} T}{\hbar \rho v_{\mathrm{s}}^2} g(E), \tag{1}$$

$$\frac{1}{\tau_{\mathrm{op}}} = \frac{\pi D_{\mathrm{op}}^2}{2\rho\omega_{\mathrm{op}}} \left(n(\omega_{\mathrm{op}}) + \frac{1}{2} \mp \frac{1}{2} \right) g(E \pm \hbar\omega_{\mathrm{op}}), \tag{2}$$

$$\begin{aligned} \frac{1}{\tau_{\mathrm{pop}}} = \frac{q^2 \omega_{\mathrm{pop}}}{4\pi\hbar v \kappa_0 \varepsilon_0} \left(\frac{\kappa_0}{\kappa_\infty} - 1 \right) \Bigg(& n(\omega_{\mathrm{pop}}) \left(1 + \frac{\hbar\omega_{\mathrm{pop}}}{E} \right)^{\frac{1}{2}} \\ & + (n(\omega_{\mathrm{pop}}) + 1) \left(1 - \frac{\hbar\omega_{\mathrm{pop}}}{E} \right)^{\frac{1}{2}} \\ & + \frac{\hbar\omega_{\mathrm{pop}}}{E} \Bigg[- n(\omega_{\mathrm{pop}}) \sinh^{-1} \left(\frac{E}{\hbar\omega_{\mathrm{pop}}} \right)^{\frac{1}{2}} \\ & + (n(\omega_{\mathrm{pop}}) + 1) \sinh^{-1} \left(\frac{E}{\hbar\omega_{\mathrm{pop}}} - 1 \right)^{\frac{1}{2}} \Bigg] \Bigg), \end{aligned} \tag{3}$$

$$\frac{1}{\tau_{\mathrm{imp}}} = \frac{n_{\mathrm{I}} q^4}{16\sqrt{2m^*}\pi\kappa_0^2\varepsilon_0^2} \left[\ln\left(1+\gamma^2\right) - \frac{\gamma^2}{1+\gamma^2} \right] E^{-\frac{3}{2}}, \tag{4}$$

where k_{B} is the Boltzmann constant, T is the lattice temperature, $g(E)$ is the density of states of the final valley, E is the carrier energy, v is the group velocity, q is the elementary charge, ε_0 is the vacuum permittivity, m^* is the effective mass, $n(\omega)$ is the Bose–Einstein distribution function, given by $n(\omega) = 1/(e^{\hbar\omega/k_{\mathrm{B}}T} - 1)$, $\gamma = 8m^* E L_{\mathrm{D}}^2/\hbar^2$, L_{D} is the Debye length, and n_{I} is the impurity concentration, taken to be $1 \times 10^{16}\,\mathrm{cm}^{-3}$. The

TABLE I: Material and simulation parameters used in this study: ρ: mass density, v_s: sound velocity, D_{ac}: acoustic phonon deformation potential, D_{op}: optical phonon deformation potential, $\hbar\omega_{op}$: optical phonon energy for intervalley scattering, $\hbar\omega_{pop}$: LO phonon energy for POP scattering, κ_0 and κ_∞: static and high-frequency relative permittivity, a, b, and E_{th}: parameters used for impact ionization rate. Carrier-dependent parameters were taken from [4] except for D_{op}.

Carrier-independent parameters

ρ [kg/m^3]	v_s [m/s]	κ_0	κ_∞	$\hbar\omega_{pop}$ [eV]	E_{th} [eV]
3211	13730	9.7	6.5	0.106	3.26

Carrier-dependent parameters

Carrier	D_{ac} [eV]	D_{op} [eV/m]	$\hbar\omega_{op}$ [eV]	a [1/s]	b
electron	11.6	6.0×10^{10}	0.085	1.0×10^{13}	4.0
hole	8.0	1.05×10^{11}	0.1	4.0×10^{13}	3.5

impact ionization rate is given by the following Keldysh formula

$$W_{ii} = a \left(\frac{E - E_{th}}{E_{th}} \right)^b \Theta(E - E_{th}), \tag{5}$$

where $\Theta(E)$ is the Heaviside step function. Table 1 shows parameters used in this study. We treat optical phonon deformation potential (D_{op}) as a constant for simplicity and use it as a fitting parameter for impact ionization coefficients.

At the crossing and anti-crossing points of the energy bands, Landau-Zener tunneling [4] was introduced to account for transitions to higher bands due to inter-band tunneling under high electric fields.

The impact ionization coefficient was calculated as

$$\alpha = \frac{n_{ii}}{\langle l \rangle}, \tag{6}$$

where n_{ii} is the number of impact ionization events, and $\langle l \rangle$ is the average distance traveled under the electric field in real space. As the number of simulated carriers increases, the value of α gradually converges toward a constant. To quantitatively assess this convergence, the standard deviation σ of α was evaluated at regular time intervals during the simulation. The simulation was conducted until the standard deviation σ fell below 10%, or until the total simulation time reached 20 ns for electrons and 10 ns for holes. The simulations were performed on a discretized three-dimensional grid in electric field space, spanning a range of electric field magnitudes and directions. This approach enabled the generation of a tabulated dataset of impact ionization coefficients as a function of the electric field vector, which can be used for device-level modeling and analysis.

In the TCAD device simulation, avalanche generation is expressed as

$$G = \frac{1}{q} \left(\alpha_n \left| \vec{j_n} \right| + \alpha_p \left| \vec{j_p} \right| \right), \tag{7}$$

where $\vec{j}$ represents the current density, with subscripts n and p referring to electrons and holes, respectively. Although α is typically modeled as a function of the electric field, in this study we applied interpolation of α values from a table obtained via FBMC, based on the local electric field. To evaluate the proposed avalanche generation model in comparison with conventional models, we simulated the reverse I–V characteristics of a diode and assessed the difference in breakdown voltage as a key performance indicator for power devices.

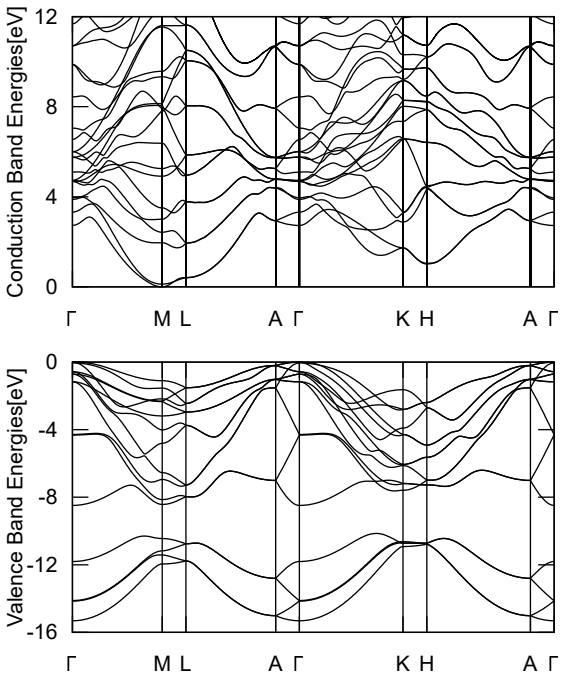

Fig. 1: The conduction and valence band structures calculated in this study.

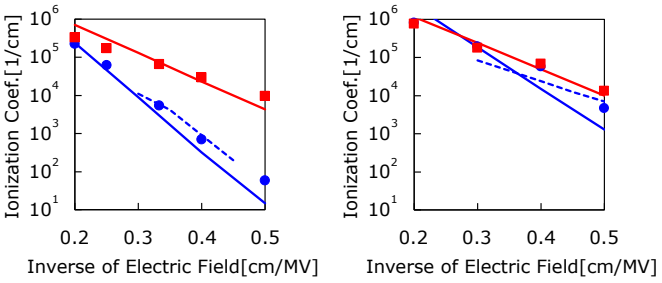

(a) electron (b) hole

Fig. 2: Impact ionization coefficients along $\langle 0001 \rangle$ (blue) and $\langle 11\bar{2}0 \rangle$ (red), calculated in this study (markers), are compared with experimental data from Hatakeyama [5] (solid lines) and Niwa [6] (dashed line).

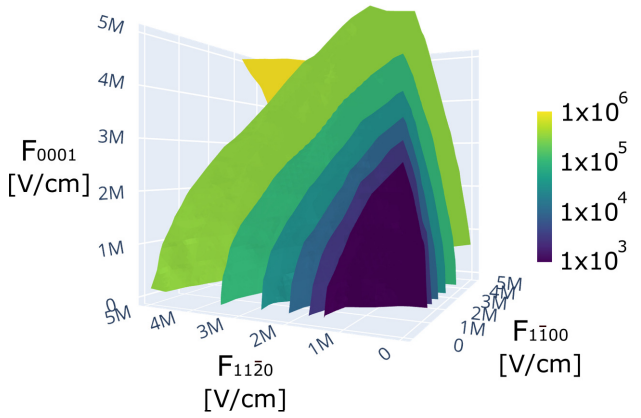

(a) electron

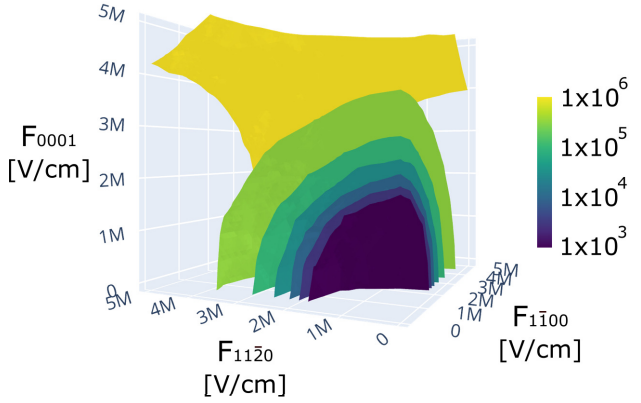

(b) hole

Fig. 3: Isosurface of impact ionization coefficients in 3D electric field space for electrons and holes, calculated using FBMC. The unit is [1/cm].

III. Results and Discussion

Figure 1 shows the electronic band structure calculated in this study. Figure 2 compares the impact ionization coefficients along the ⟨0001⟩ and ⟨11$\bar{2}$0⟩ directions obtained from FBMC with experimental results, showing good agreement. Figure 3 presents the impact ionization coefficients for electrons and holes in arbitrary directions, which, to the best of our knowledge, have not been reported before. Our results indicate strong anisotropy only in the ⟨0001⟩ direction for electrons, while others show weak anisotropy.

The strong anisotropy of the impact ionization coefficients for electrons in the ⟨0001⟩ direction can be explained by the band structure and the anisotropy of energy gain during free flight. Figure 4 shows a histogram of energy gain during free flight in the second conduction band. Under an electric field along the ⟨0001⟩ direction, the energy gain is significantly smaller compared to other directions, and the scatter plot of electron wave vectors at the end of the free flight shows that low-energy electrons are confined around the M point.

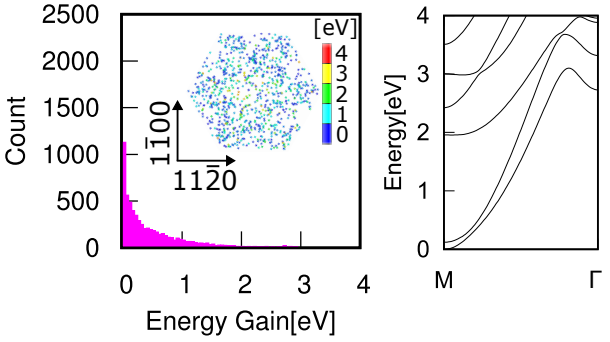

(a) $F_{1\bar{1}00}$

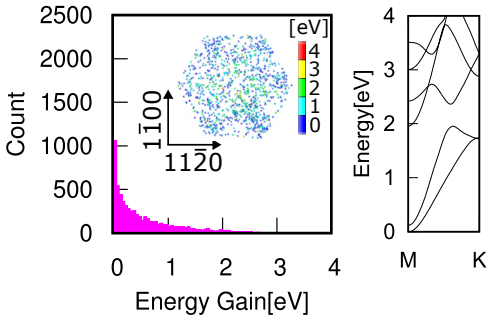

(b) $F_{11\bar{2}0}$

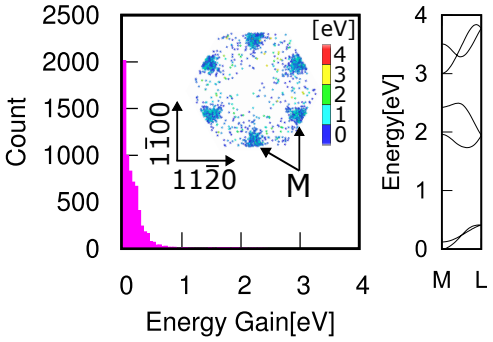

(c) F_{0001}

Fig. 4: Histograms of energy gain during free flight under a 5 MV/cm electric field. Scatter plots show the wave vector distribution in the first Brillouin zone at the end of free flight, with colors indicating energy gain. The corresponding band structures in each direction are also shown. The simulation time was set to 0.5 ps.

Figure 5 compares the contour plots of the impact ionization coefficients of electrons in the ⟨0001⟩ and ⟨11$\bar{2}$0⟩ directions obtained from FBMC with those from the conventional model [7]. After adjusting the parameters of the conventional model so that the impact ionization coefficients in the ⟨0001⟩ and ⟨11$\bar{2}$0⟩ directions match, a difference of approximately half an order of magnitude appears in the off-axis impact ionization coefficients, resulting in more accurate values.

Figure 6 shows the distribution of impact ionization coefficients at the corner of the pn junction of a diode under

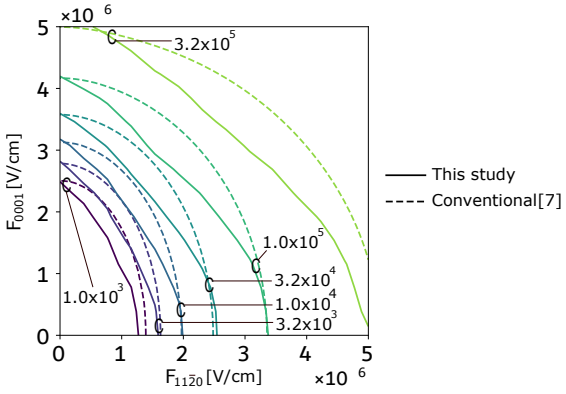

Fig. 5: Contour plot of impact ionization coefficients in the 2D electric field space defined by the $\langle 0001 \rangle$ and $\langle 11\bar{2}0 \rangle$ directions. The solid line represents the results of this study, while the dashed line corresponds to a conventional model based on [7]. The unit is [1/cm].

reverse bias. The difference in off-axis impact ionization coefficients shown in Figure 5 is accurately reproduced. As shown in Figure 7, the new model yields a breakdown voltage approximately 10% lower than that of the conventional model. This significantly affects the accuracy of breakdown voltage prediction, particularly in regions where the electric field becomes concentrated in off-axis directions due to curved device geometries, such as the corner of a pn junction or the bottom of a trench. In such cases, anisotropic modeling of impact ionization becomes essential.

Unlike previous models, the model developed in this study is not constrained to specific functional forms, allowing for accurate representation of complex distributions. Furthermore, updating the FBMC results enables coverage of a wider range of electric fields.

IV. Conclusion

A novel avalanche generation model was developed using impact ionization coefficients obtained from high-field transport in 4H-SiC, based on multiscale modeling with DFT and FBMC. This framework bridges atomic-scale and device-level physics, enabling accurate simulations and offering deep physical insights. Furthermore, it serves as a powerful tool for uncovering previously unexplored phenomena, paving the way for predictive modeling in wide-bandgap semiconductor devices.

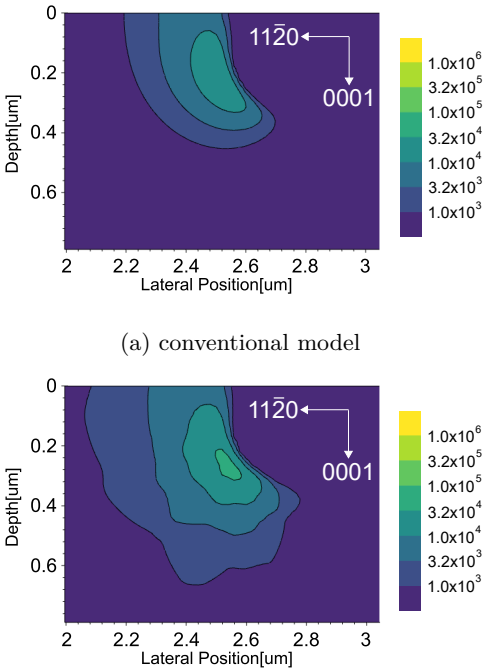

(a) conventional model

(b) this study

Fig. 6: The distribution of impact ionization coefficients at the corner of the pn junction in a diode under a 400 V reverse bias, for both electrons and holes. The unit is [1/cm].

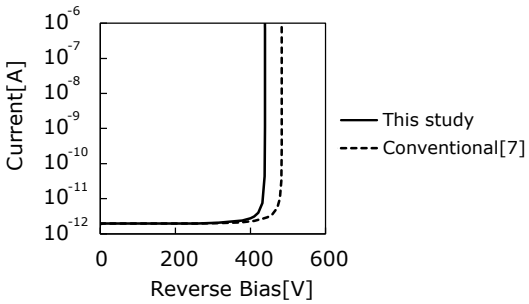

Fig. 7: Results of TCAD device simulation of the reverse I–V characteristics of a diode. The solid line represents the results of this study, while the dashed line corresponds to a conventional model based on [7].

References

[1] P. Giannozzi *et al.*, "QUANTUM ESPRESSO: a modular and open-source software project for quantum simulations of materials," *Journal of Physics: Condensed Matter*, vol. 21, no. 39, p. 395502, 2009.

[2] D. R. Hamann, "Optimized norm-conserving Vanderbilt pseudopotentials," *Physical Review B*, vol. 88, no. 8, p. 085117, 2013.

[3] G. Pizzi *et al.*, "Wannier90 as a community code: new features and applications," *Journal of Physics: Condensed Matter*, vol. 32, no. 16, p. 165902, 2020.

[4] H. Tanaka *et al.*, Theoretical study on high-field carrier transport and impact ionization coefficients in 4H-SiC, *Materials Science in Semiconductor Processing*, vol. 173, 2024, Art. no. 108126.

[5] T. Hatakeyama *et al.*, "Impact ionization coefficients of 4H silicon carbide," *Applied Physics Letters*, vol. 85, no. 8, pp. 1380–1382, 2004.

[6] H. Niwa *et al.*, "Ultrahigh-voltage SiC devices with improved forward characteristics," *IEEE Transactions on Electron Devices*, vol. 62, no. 10, pp. 3326–3333, 2015.

[7] T. Hatakeyama *et al.*, "Physical modeling and scaling properties of 4H-SiC power devices," in *Proc. Int. Conf. Simulation of Semiconductor Processes and Devices (SISPAD)*, Tokyo, Japan, 2005, pp. 171–174.